Epidermal TRPM8 channel isoform controls the balance between keratinocyte proliferation and differentiation in a cold-dependent manner

Gabriel Bidaux[a,b,1,2], Anne-sophie Borowiec[a], Dmitri Gordienko[a,3,4], Benjamin Beck[a,5], George G. Shapovalov[a], Loïc Lemonnier[a], Matthieu Flourakis[a,6], Matthieu Vandenberghe[a], Christian Slomianny[a], Etienne Dewailly[a], Philippe Delcourt[a], Emilie Desruelles[a], Abigaël Ritaine[a], Renata Polakowska[c], Jean Lesage[d], Mounia Chami[e], Roman Skryma[a,4], and Natalia Prevarskaya[a,2,4]

[a]Inserm U-1003, Equipe Labellisée par la Ligue Nationale Contre le Cancer et LABEX (Laboratoire d'excellence), Université Lille1, 59655 Villeneuve d'Ascq, France; [b]Equipe Biophotonique Cellulaire Fonctionnelle, Laboratoire de Physique des Lasers, Atomes & Molécules, Parc Scientifique de la Haute Borne, 59655 Villeneuve d'Ascq, France; [c]Inserm U837, Jean-Pierre Aubert Research Center, Institut pour la Recherche sur le Cancer de Lille, 59045 Lille, France; [d]Université Lille Nord de France, Unité Environnement Périnatal et Croissance, EA (Equipe d'Acceuil) 4489, Equipe Dénutritions Maternelles Périnatales, Université Lille 1, 59655 Villeneuve d'Ascq, France; and [e]Institut de Pharmacologie Moléculaire et Cellulaire, UMR7275 CNRS/Univerité de Nice Sophia-Antipolis, Équipe Labellisée "Fondation pour la Recherche Médicale" 1 and "Excellence Laboratory Distalz," 06560 Valbonne, France

Deviation of the ambient temperature is one of the most ubiquitous stimuli that continuously affect mammals' skin. Although the role of the warmth receptors in epidermal homeostasis (EH) was elucidated in recent years, the mystery of the keratinocyte mild-cold sensor remains unsolved. Here we report the cloning and characterization of a new functional epidermal isoform of the transient receptor potential M8 (TRPM8) mild-cold receptor, dubbed epidermal TRPM8 (eTRPM8), which is localized in the keratinocyte endoplasmic reticulum membrane and controls mitochondrial Ca^{2+} concentration ($[Ca^{2+}]_m$). In turn, $[Ca^{2+}]_m$ modulates ATP and superoxide ($O_2^{\bullet-}$) synthesis in a cold-dependent manner. We report that this fine tuning of ATP and $O_2^{\bullet-}$ levels by cooling controls the balance between keratinocyte proliferation and differentiation. Finally, to ascertain eTRPM8's role in EH in vivo we developed a new functional knockout mouse strain by deleting the pore domain of TRPM8 and demonstrated that eTRPM8 knockout impairs adaptation of the epidermis to low temperatures.

eTRPM8 | cold | epidermal homeostasis | calcium | mitochondria bioenergetics

The skin epidermis provides a protective barrier that guards the body against an uncongenial environment. Under the influence of a variety of ambient factors the skin epidermis undergoes continuous regeneration through so-called epidermal homeostasis (EH): the fine-tuning of the balance between proliferation, directional migration, differentiation, and death of keratinocytes. EH involves complex molecular and chemical pathways, regulating dynamic and continuous transition of keratinocytes from the proliferating state in the basal layer to the nonproliferating state in the suprabasal layer before the beginning of the differentiation in the stratum spinosum and stratum granulosum. The terminal differentiation step, characterized by keratinocyte death, transforms keratinocytes into corneocytes, which form the waterproof, mechanically resistant sheath of the stratum corneum (1).

Deviation of the ambient temperature is one of the most important stimuli that constantly affect mammals' skin. At ambient temperatures from +10 °C to +30 °C, the unprotected human skin temperature settles at mean steady-state values within the range of +24 °C to +33 °C, respectively (2). Temperature is perceived by thermoreceptors, the ion channels that belong to the transient receptor potential (TRP) superfamily (for review see ref. 3). Of these, TRPV1 and TRPV2 are activated by heat (above 42 °C and above 52 °C, respectively) (4), whereas TRPM8 and likely TRPA1 are activated by mild (5, 6) and noxious (7–9) cold, respectively. Heat-stimulated keratinocytes have been shown to secrete ATP (10) and, taking into account that purinergic receptors are expressed in keratinocytes (11), TRPV3 is involved in a paracrine heat-

induced regulator of EH. Surprisingly, Grifford et al. recently reported that local heating of human skin does not result in accumulation of interstitial ATP (12), which refutes the significance of TRPV thermoreceptors in normal temperature-dependent EH. TRPV3 also was suggested to be important for corneocyte formation through Ca^{2+}-dependent activation of cross-linking enzymes such as transglutaminase (13–15). Apart

Significance

Epidermis, the outer layer of skin, is a protective barrier and a sensing interface. Although deviation of the ambient temperature is one of the most ubiquitous stimuli affecting the skin, the influence of mild cold on epidermal homeostasis is not well understood. Using a large range of techniques, we identified a novel mild-cold sensor protein in keratinocytes and demonstrate its location in the membrane of the endoplasmic reticulum, a major calcium store of the cell, which forms a Ca^{2+}-permeable ion channel. Activation of this channel links the Ca^{2+} release to mitochondrial Ca^{2+} uptake and, thereby, modulates synthesis of ATP and superoxide involved in control of epidermal homeostasis. Molecular inactivation of this mild-cold sensor protein in mice impairs normal epidermal homeostasis.

from heat-activated TRP, no successful attempt to elucidate the role of cold-sensitive TRP channels in EH has been reported yet. The range of thermoactivation of TRPM8 channel fits well with human unprotected skin temperature, +24 °C to +33 °C (5, 6). Apart from the observation that topical application of TRPM8 chemical agonists can improve epidermal regeneration (16), no solid evidence for the expression of functional TRPM8 in epidermal keratinocytes has been presented yet and no alterations in epidermal homeostasis have been reported in $trpm8^{-/-}$ null mutant mice suppressing the full-length TRPM8 cold receptor (17, 18). However, suppression of the full-length TRPM8 expression does not necessarily affect expression of TRPM8 isoforms (19).

Here we report the cloning and characterization of a new four-transmembrane domain epidermal isoform of the TRPM8 cold receptor channel, dubbed epidermal TRPM8 (eTRPM8). We demonstrate that eTRPM8 is localized and functions in the keratinocyte endoplasmic reticulum (ER) membrane where its activation within ER–mitochondria contact sites sustains mitochondrial Ca^{2+} uptake, thus affecting mitochondrial Ca^{2+} concentration ($[Ca^{2+}]_m$). In turn, $[Ca^{2+}]_m$ modulates ATP and superoxide ($O_2^{•-}$) synthesis in a cold-dependent manner. We report that this fine-tuning of ATP and $O_2^{•-}$ levels by cooling temperatures controls the balance between proliferation and differentiation of keratinocytes. Finally, to ascertain eTRPM8's role in EH in vivo we developed a new functional knockout (KO) mouse line by deleting the active pore domain in all TRPM8 channel isoforms and demonstrated that eTRPM8 knockout impairs the epidermis adaptation to low temperatures and general skin homeostasis.

Results and Discussion

Novel TRPM8 Isoform Identified in Human Keratinocytes Is Composed of Four Transmembrane Domains.
Using differential PCR screenings to characterize TRPM8 mRNA in human keratinocytes, we found that in both the HaCaT human keratinocyte cell line and human normal epidermal keratinocytes (hNEKs) TRPM8 mRNA is 5′ truncated. Indeed, in both cell types, PCR analysis reported the product of amplification of the pore-encoding mRNA region, but not exons 2–7 or exons 11–14 in the 5′ region of TRPM8 mRNA (Fig. 1A). Controls on primary prostate epithelial cells (PrPEs) were positive for all three regions tested, which validates the primers used for the detection of the classical TRPM8 mRNA. This demonstrates that the classical full-length TRPM8 is not expressed in keratinocytes. This conclusion was confirmed further by Western blot analysis that demonstrates the classical TRPM8 (the 130-kDa doublet) in total protein extract from human prostate, but not from hNEK and HaCaT cells (Fig. 1B). The 5′-RACE PCR, performed from pore-encoding exon 20, revealed a new alternate starting exon, labeled 15a. It was located upstream and was adjacent to core exon 15, which was renamed 15b, respectively (Fig. S1A). Internal quality control for the RACE PCR was performed with the cloning of the 5′ extremity of classical TRPM8 mRNA in human prostate. We succeeded in amplifying 2,900 bp (GenBank accession no. KC692993) and improved the definition of the first transcribed nucleotide (+1) of the TRPM8 mRNA, because we detected 10 additional bases upstream of the published +1 (NM_024080.4). This makes the new +1 nucleotide located 25 bases downstream of the TATAA box. Although the previously published +1 nucleotide was identified as located 35 bases downstream (20), this does not match the consensus distance between the TATAA box and +1 (from 15 bp to 25 bp). As presented in Fig. S1A, two sequences were cloned from hNEK mRNA: an alternate TRPM8 mRNA from exon 15a to exon 26, labeled TRPM8(15a) (GenBank accession no. KC692994), and a splice variant of this alternate mRNA with skipping of exon 16, labeled TRPM8(15a/δ16) (GenBank accession no. KC692995). TRPM8(15a) was found in human prostate, testis, skin, and brain, whereas TRPM8(15a/δ16) was detected in human skin and colon (Fig. 1C). Quantification of TRPM8(15a) mRNAs in keratinocytes demonstrated a similarly low level of the mRNAs in the HaCaT cell line and basal hNEKs, whereas induction of hNEKs (Materials and Methods) was associated with a significant increase in the level of TRPM8(15a) mRNAs (Fig. S1B). Furthermore, we verified eTRPM8 expression in human epidermis with in situ hybridization and immunohistofluorescence. In situ hybridization showed a positive detection of the pore-encoding region in epidermis, specifically with the antisense probe (Fig. S1C). Immunodetection of eTRPM8 with the antibody against the P loop of the TRPM8 channel confirmed epidermis-specific expression of eTRPM8 showing a marked increase of the channel expression in differentiated layers of epidermis (Fig. 1D).

Surprisingly, the putative ORFs of the two mRNAs were quite similar; however, TRPM8(15a/δ16) revealed an additional longer ORF (Fig. S1A). After quantification of TRPM8(15a) mRNA and TRPM8(15a/δ16) mRNA intensities with a gel imager, TRPM8(15a) in skin was about four times more expressed than its splice form, and we focused on TRPM8(15a) and defined its putative protein as epidermal TRPM8 (eTRPM8). Note that 5′ truncation removes the first 14 exons (Fig. S1A), which indicates that the two longest, putative ORFs encode four-transmembrane domain (4-TD) proteins, including TD3–6 and the P-loop–forming pore segment, with molecular masses of 40.94 kDa and 35.77 kDa, respectively (Fig. S1D). Immunoblotting of wild-type (WT) eTRPM8 or HA-tagged eTRPM8 expressed in HEK cells revealed a major 39- to 40-kDa doublet and a minor 35- to 36-kDa doublet (Fig. 1E), which are referred to as eTRPM8-40 and eTRPM8-36, respectively. Native eTRPM8 expression was confirmed in two independent hNEK samples (Fig. 1F) and it should be noted that a rather low level of protein expression correlates with a low level of eTRPM8 mRNA in keratinocytes.

Cold (<32 °C) and cooling agents, such as menthol and icilin, activate the TRPM8 channel (5, 6). Although the precise position of the menthol and icilin binding sites in classical TRPM8 is not yet clearly identified, there is growing evidence that both agonists interact with transmembrane domains 3 and 4 of the channel (reviewed in ref. 21). This indirectly suggests that both agonists may bind to eTRPM8. In addition, because the cold sensor domain is located in the carboxy-terminus of classical TRPM8 (22), it is likely that eTRPM8 may function as a cold-sensitive protein. Nevertheless, no changes in transmembrane ion currents, recorded under whole-cell voltage clamp in eTRPM8-expressing HEK cells, were detected in response to cold, menthol, or icilin. This ruled out eTRPM8 as a plasma membrane functional channel. Based on our previous findings (19) we hypothesized that, similarly to TRPM8 in prostate cancer cells, eTRPM8 in keratinocytes may function as the ER Ca^{2+}-release channel. To test this hypothesis, we first conducted double immunostaining of eTRPM8 and the ER protein calnexin. This revealed (Fig. S2) that eTRPM8 clusters coincide with the ER elements in CTL and eTRPM8-overexpressing HaCaT cells and in hNEKs. Because eTRPM8 is expressed in the ER of keratinocytes, to measure eTRPM8-mediated single-channel current we conducted patch-clamp recording on the giant unilamellar vesicles (GUVs) containing the proteins extracted from the ER membrane fractions of HEK293 cells expressing eTRPM8 (Fig. 1 G–L).

Biophysical properties of the single-channel activity measured under these conditions were characteristic of the TRPM8 channel: (i) single-channel conductance of 63.1 ± 2.4 pS and dependence of P_{open} on applied voltage at 20 °C, basal and in response to menthol, as well as at 37 °C (n = 33, 37, and 5); (ii) sensitivity to all currently known specific activators and inhibitors of TRPM8; and (iii) PiP_2 dependence. The single-channel current was activated by 10 μM icilin (n = 16), 500 nM ws-12 (23) (n = 18), or 200 μM menthol (n = 31); required the presence of PiP_2 in GUVs; and was blocked by 10 μM BCTC (n = 13). Stimulation with these activators of the patches made to the GUVs prepared from cells expressing the empty vector (n = 290) or nonfunctional mutant eTRPM8(Y148A) (n = 258) failed to induce the single-channel activity.

Thus, we have cloned a new kind of TRP channel, eTRPM8, which, in contrast to all previously known members of the TRP family, has the 4-TD structure. Furthermore, we demonstrated
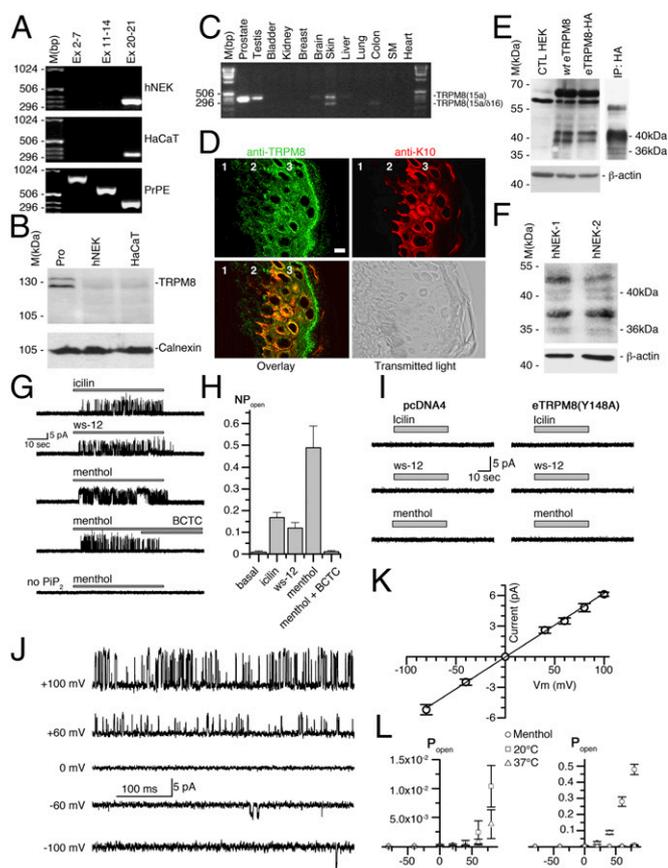
Fig. 1. Trpm8 gene encodes alternate TRPM8 mRNA variants and their associated proteins in human keratinocytes. (*A*) Representative PCR finger-printing (*n* = 5) revealed expression of the pore-encoding region (exons 20 and 21) in the keratinocyte HaCaT cell line, in human normal epidermal keratinocytes (hNEK), and in primary culture of human prostate epithelial (PrPE) cells. Note that segments from exons 2–7 and from exons 11–14, encoding the cytosolic N terminus of the TRPM8 channel, were detected in PrPE cells but not in keratinocytes. (*B*) Representative immunoblotting (*n* = 3) of 100 μg total protein extracts from human prostate (Pro), human normal epidermal keratinocytes (hNEK), and HaCaT cell line. A classical full-length TRPM8 channel (126–128 kDa) was detected with rabbit anti-TRPM8 antibody (Alomone Laboratories; batch from 2009). Calnexin protein was used as a reporter of equal loading. (*C*) Full-length PCR illustrates human tissue profiling of alternate TRPM8(15a) transcripts (*n* = 3). (*D*) The gallery shows fluorescent confocal images of human female breast skin sections (*n* = 3) with immunostained eTRPM8 (*Upper Left*, green) and keratin 10 (*Upper Right*, red) and their overlay (*Lower Left*) and corresponding transmitted light image (*Lower Right*). Numbers on the images depict the following: 1, dermis; 2, basal layer of epidermis; and 3, spinal and granular layers of epidermis. (Scale bar: 5 μm.) (*E*) Wild-type eTRPM8 and HA-tagged eTRPM8 (WT eTRPM8 and eTRPM8-HA, respectively), detected with anti-TRPM8 antibody in total protein extract from HEK cells, show a strong doublet at 39–40 kDa and much weaker doublet at 35–36 kDa. β-actin was used as a control of the protein loading. Immunoprecipitation with anti-HA antibody followed by immunoblotting with anti-TRPM8 antibody (*E, Right*, IP: HA) confirms specificity of both doublets and invalidates nonspecific bands between 55 kDa and 70 kDa. The same results were obtained in three independent samples. (*F*) Native eTRPM8 protein detected with anti-TRPM8 immunoblotting in two independent samples (hNEK-1 and -2) of the induced hNEKs. β-actin was used as a control of the protein loading. (*G* and *H*) Sample activity of eTRPM8 in response to application of 10 μM icilin, 500 nM ws-12, and 200 μM menthol, as well as inhibition by 10 μM BCTC, with levels of eTRPM8 activity summarized in *H*. (*I*) Typical records upon application of icilin, ws-12, and menthol to liposomes prepared from cells expressing the nonfunctional pore mutant eTRPM8(Y148A) or transfected with empty vector (pcDNA44). (*J*) Sample activity of ws-12–activated eTRPM8 at different potentials, indicated at left. Note the characteristic dependence of open probability on the command potential. (*K*) Dependence of the amplitude on command voltage. Straight line presents a linear fit

that keratinocytes express eTRPM8 instead of classical TRPM8, which raised the question about its role in epidermal homeostasis.

Functional TRPM8 Knockout Impairs Skin Differentiation in Mouse. Several trpm8$^{-/-}$ mouse strains have been generated by deletion of either the first translated exon or exons in the first half of the TRPM8 sequence (17, 18). These mutations, however, did not target the pore region and, therefore, failed to suppress eTRPM8 expression and activity. In contrast, based on our previous detection of amino-terminal truncated TRPM8 isoforms (19), we have designed a functional KO mouse line by deleting exons 18, 19, and 20, which encode the active pore domain (Fig. 2*A* and Fig. S1*A*). Here we assessed the expression of mouse orthologous eTRPM8. PCR amplification of TRPM8(15a) was successfully achieved from exon 16 to exon 23 in total mRNA extracts (Fig. 2*B*), not only from skin sections of wild-type mice but also from primary culture of wild-type mouse keratinocytes (WT mPK) grown with 2% FCS + 1.8 mM Ca^{2+} (24). This implies that eTRPM8, detected in the skin sections, is hosted by keratinocytes. Moreover, the lack of amplification products for exons 14–23 is indicative of truncation of the first half of the 5′ exon characteristic of the eTRPM8 sequence. Specificity of TRPM8 detection was validated in the samples from TRPM8 KO mice that do not express TRPM8. Finally, we checked eTRPM8 protein expression in freshly isolated mouse keratinocytes (FIMKs) and detected a doublet of protein near 39 kDa from WT cells, which was not present in FIMK from trpm8$^{-/-}$ mice (Fig. 2*C*).

To address involvement of eTRPM8 in EH we tested whether eTRPM8 KO would impair EH. Immunohistofluorescence analysis revealed a significant decrease of the number of proliferating cell nuclear antigen (PCNA) positive cells in trpm8$^{-/-}$ basal/suprabasal compartments (B/SbS) labeled with keratin 5 (K5) (Fig. 2 *D* and *E*). This suggests that the proliferation level of the stratum basale (SB) is impaired in eTRPM8 KO epidermis. Because suppression of the channel pore region abolishes the activity of both eTRPM8 and classical TRPM8, to eliminate any possible involvement of the TRPM8 KO in the measurements (even though we obtained no evidence for the TRPM8 expression in keratinocytes) we conducted additional control experiments on the trpm8$^{-/-}$ (DJ) mouse strain, where only classical TRPM8, but not eTRPM8, is suppressed (Fig. 2*F*). No changes in the proportion of PCNA positive cells in comparison with that in WT mice were detected in these experiments (Fig. 2*G*). Furthermore, measurements of the thickness of the different epidermal layers (Fig. 2 *D* and *G*) revealed a significant increase of B/SbS, no change in stratum spinosum (SS) plus stratum granulosum (SG), and a significant decrease of the SG. These data indicate that the SS thickness is increased in proportion to the decrease of the SG thickness, so that total thickness of the two layers remains unchanged. The observed alterations were further confirmed by assessing the percentage of FIMKs positive for a specific epidermal layer marker (Fig. 2*H*). We have found that FIMKs from trpm8$^{-/-}$ mice were enriched in the number of basal keratin 5 (K5)-positive, keratin 10 (K10)-negative (K5$^+$/K10$^-$) proliferating cells, as well as in involucrin (INV)-positive, filaggrin (FLG)-negative (INV$^+$/FLG$^-$) late spinosum cells, but they were slightly depleted of filaggrin-positive (INV$^+$/FLG$^+$) granulosum cells, compared with the WT FIMKs. Finally, consistent with the decrease of proliferation and increase in late differentiation, we have detected the decrease in the thickness of the stratum corneum (SC) in the skin samples of different body regions from trpm8$^{-/-}$ mice: snout, palm, backskin, and tail (Fig. 2*I*).

Altogether, our data in the trpm8$^{-/-}$ mouse model demonstrated an impairment of EH, which was characterized by the decrease of proliferation rate and accumulation of keratinocytes

yielding the mean channel conductance of 63.1 ± 2.4 pS. (*L*) Comparison of P$_{open}$ vs. voltage curves at 20 °C and 37 °C (*Left*) and basal and menthol stimulated at 20 °C (*Right*). Individual points show mean ± SEM values at the indicated voltages.
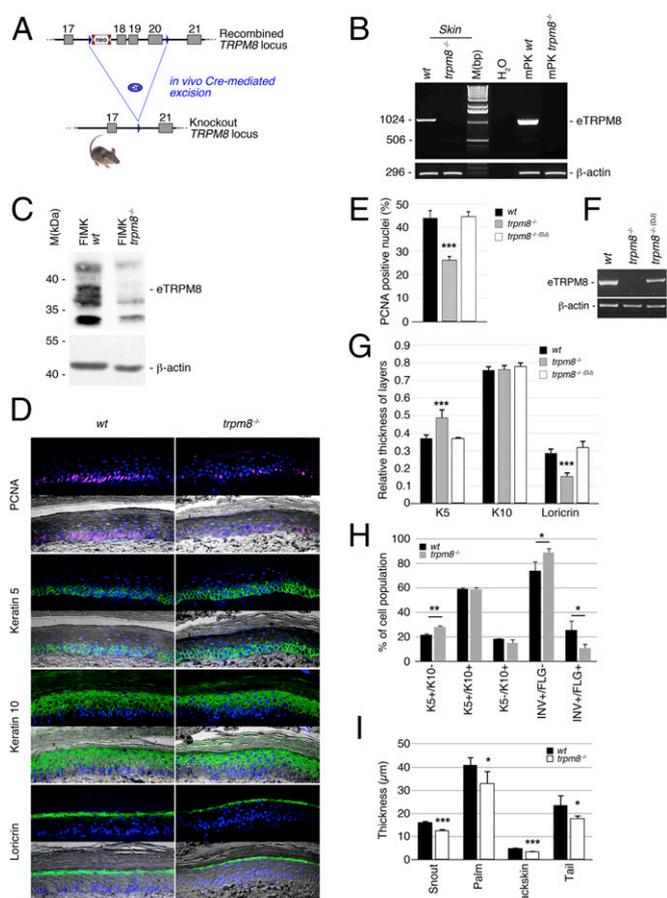
Fig. 2. Epidermal TRPM8 isoform (eTRPM8) ablation in mouse epidermis partially impairs epidermal homeostasis. (*A*) Schematic representation of the strategy used to establish the *trpm8* $^{-/-}$ mouse line. (*B*) PCR amplification from exon 16 to exon 22 demonstrates expression of mouse eTRPM8 mRNA in wild type (WT) skin as well as in mPKs derived from WT mouse skin and grown with 2% FCS and 1.8 mM Ca^{2+} (mPK WT). Note that no eTRPM8 expression was detected in keratinocytes derived from *trpm8* $^{-/-}$ mouse skin (mPK *trpm8* $^{-/-}$) (*n* = 3). (*C*) Immunoblotting shows ~38 kDa protein in the skin of WT but not *trpm8* $^{-/-}$ mice (one of four readings for each mouse strain). β-actin was used as a control of the protein loading. (*D*) Representative immunohistofluorescence images of WT and *trpm8* $^{-/-}$ mouse palm skin reveal a decreased number of cycling cells in *trpm8* $^{-/-}$ epidermis (reported by PCNA) and a thicker granular layer (reported by loricrin, LN). (*E*) Bar diagram compares fractions of the cells with PCNA-positive nuclei in the keratin 5 (K5)-positive cell compartment counted in the images of skin sections of five WT mice, seven *trpm8* $^{-/-}$ mice, and five *trpm8* $^{-/- (DJ)}$ mice (lacking full-length TRPM8 channel only). Note that the *trpm8* $^{-/-}$ mouse skin section (*D*) has a thicker basal layer (K5-positive cells) but a thinner granular layer (LN-positive cells), whereas the total thickness of SS + SG remains unaltered. (*F*) PCR amplification from exon 16 to exon 22 demonstrates expression of mouse eTRPM8 mRNA in skin sections of WT mice, *trpm8* $^{-/-}$ mice, and *trpm8* $^{-/- (DJ)}$ mice. (*G*) Bar diagram plot compares relative thickness (*Materials and Methods*) of K5-, K10-, and LR-positive compartments in five WT mice, seven *trpm8* $^{-/-}$ mice, and five *trpm8* $^{-/- (DJ)}$ mice. (*H*) Distribution of keratinocyte phenotypes in the suspension of cells, freshly isolated from the back skin samples of five WT and five *trpm8* $^{-/-}$ mice, was measured with flow cytometry and compared. The phenotypes detected include basal cells (K5+/K10−), suprabasal and early spinal cells (K5+/K10+), late spinal cells (K10+/INV+/FLG−), and granular cells (INV+/FLG+). (*I*) Thickness of corneosum stratum (CS) was measured in trichrome-stained slides of paraffined skin samples obtained from the different skin regions (as indicated) and compared for five WT and five *trpm8* $^{-/-}$ mice.

in basal/suprabasal layers and early SS paralleled with a partial depletion of the cells in SG and SC. We therefore have concluded that eTRPM8 is an important modulator of EH. This prompted us to study molecular mechanisms of eTRPM8-dependent EH regulation.

eTRPM8 Is the ER Ca^{2+}-Release Channel, Activity of Which Affects $[Ca^{2+}]_m$. To assess immediate consequences of eTRPM8 activation in keratinocytes, we monitored menthol-induced changes of the ionized Ca^{2+} concentration in cytosol ($[Ca^{2+}]_c$) and mitochondria ($[Ca^{2+}]_m$), using fluorescence confocal imaging. In these experiments, to eliminate a possible contribution of capacitative Ca^{2+} entry and, thereby, to enable the detection of Ca^{2+} flow among intracellular compartments only, external solution, containing 70 μM Ca^{2+}, was supplemented with 10 μM La^{3+} (25). Changes of $[Ca^{2+}]_c$ and $[Ca^{2+}]_m$ in response to external application of 200 μM menthol were simultaneously monitored at 37 °C, using fluo-4 and rhod-2, respectively. The $[Ca^{2+}]_c$ and $[Ca^{2+}]_m$ transients detected in mPKs from wild-type mice (Fig. 3*A*) were virtually abolished (Fig. 3*C*) in mPKs from *trpm8* $^{-/-}$ mice (Fig. 3*B*), whereas the transients observed in control HaCaT cells (Fig. 3*D*) were significantly augmented (Fig. 3*F*) following eTRPM8 overexpression (Fig. 3*E*). Induction (*Materials and Methods*) of hNEKs also increased the amplitude of both $[Ca^{2+}]_c$ and $[Ca^{2+}]_m$ transients (Fig. S3 *A* and *B*), which correlates with elevation of eTRPM8 protein expression (Fig. 1*D*). The sensitivity of eTRPM8 to menthol, icilin, cold, and WS-12 (synthetic TRPM8 agonist) was further confirmed by wide-field microscopy of the fura-2 responses (Fig. S3 *C* and *D*). Moreover, to verify the origin of Ca^{2+}, giving rise to $[Ca^{2+}]_c$ and $[Ca^{2+}]_m$ transients, we monitored icilin-induced changes of the ER Ca^{2+} concentration ($[Ca^{2+}]_{ER}$) in permeabilized HaCaT cells. This revealed (Fig. S3*E*) that decrease of $[Ca^{2+}]_{ER}$ in response to 10 μM icilin, observed in control HaCaT cells, was abolished following eTRPM8 knockdown (KD), achieved by transfection of HaCaT cells with shRNA targeting the eTRPM8-pore–encoding sequence (shM8). Mitochondrial origin of rhod-2 signal was confirmed by visualization of the mitochondria with MitoTracker Green FM (Fig. S2*F*).

Another line of evidence, confirming that eTRPM8 functions as a Ca^{2+}-permeable channel, was derived from the experiments on mutation of the channel pore region. We generated a pore-killer mutant of a classical TRPM8 channel by substituting tyrosine 905 with alanine that completely abolished the current through the homotetrameric channel and had a partial dominant-negative effect (Fig. S4*A*). By analogy, we created an identical pore-killer mutant for eTRPM8, eTRPM8(Y148A), and overexpressed it in HaCaT cells. In this experimental model no Ca^{2+} release from the ER and concurrent mitochondrial Ca^{2+} uptake was ever observed (Fig. S4*B*), whereas the protein expression was confirmed in Western-blot experiments. This implies that the pore-killer mutation abolishes the channel activity of eTRPM8, as it does in classical TRPM8 (Fig. S4*A*), and further confirms that the ER Ca^{2+} release leading to mitochondrial Ca^{2+} uptake is mediated via eTRPM8 (Fig. S4*B*).

This suggests tight coupling between the ER and mitochondria, which facilitates mitochondrial Ca^{2+} uptake either by robust increase of Ca^{2+} concentration in the ER mitochondria "nanodomains" (26) or via direct "Ca^{2+} tunneling" from the ER to mitochondria (27). Immunofluorescence detection of native eTRPM8 in HaCaT cells, overexpressing DsRed targeted to mitochondria, revealed that eTRPM8 foci surround mitochondria (Fig. 3*G*). More evidence that eTRPM8-enriched ER elements are tightly coupled to mitochondria was obtained from the analysis of motility of the ER elements and mitochondria in living HaCaT cells (Movies S1 and S2). This revealed extremely high correlation in the step-by-step displacements of the ER element, visualized either with Brefeldin A BODIPY staining (Fig. 3*H*; *n* = 8) or following eTRPM8-mTurquoise2 expression (Fig. 3*I*; *n* = 10), and the adjacent mitochondrion. The co-ordinated motility of the organelles indicates that mitochondria are "anchored" to the adjacent eTRPM8-enriched ER elements.

Taken together, the above results imply that eTRPM8 is an ER functional channel, which, forming calcium nanodomains, couples the ER Ca^{2+} release to mitochondrial Ca^{2+} uptake in keratinocytes. We therefore analyzed the downstream molecular events engaged by eTRPM8 activation.
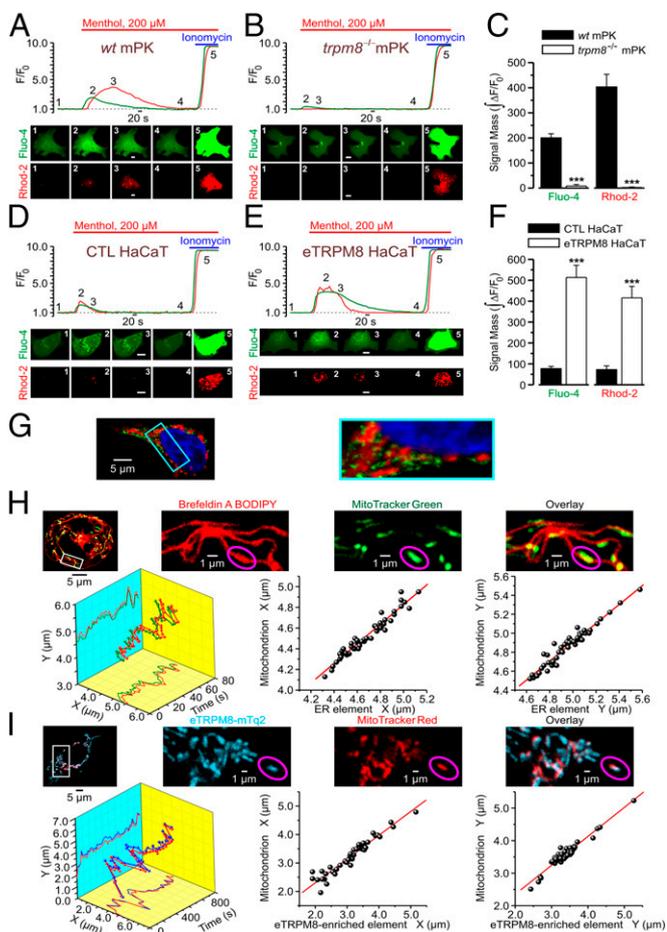
Fig. 3. eTRPM8 couples Ca^{2+} release from the ER to mitochondrial Ca^{2+} uptake. Changes of Ca^{2+} concentration in cytosol ($[Ca^{2+}]_c$) and mitochondria ($[Ca^{2+}]_m$) in response to external application of 200 μM menthol were monitored using x-y time series imaging of fluo-4 and rhod-2 fluorescence, respectively, in primary cultures of (A) wild-type mouse keratinocytes (WT mPK) and (B) trpm8 $^{-/-}$ mouse keratinocytes (trpm8 $^{-/-}$ mPK) and in (D) control HaCaT cells (CTL HaCaT) and (E) HaCaT cells overexpressing eTRPM8 (eTRPM8 HaCaT). The plots show the time course of normalized fluorescence (F/F_0) of fluo-4 (green traces) and rhod-2 (red traces). The galleries below the plots demonstrate the images of fluo-4 and rhod-2 fluorescence (as indicated), captured at the moments depicted by the numbers on the plots, respectively. (Scale bar: 10 μm.) To eliminate capacitative Ca^{2+} entry, an external solution, containing 70 μM Ca^{2+}, was supplemented with 10 μM La^{3+}. To estimate the load of the Ca^{2+}-sensitive indicators, the cells were exposed to 2.5 μM of ionomycin at the end of each experiment. Bar diagram plots compare masses, $\int \Delta F/F_0$, of the fluo-4 and rhod-2 signals (as indicated) during the period between application of menthol and application of ionomycin in (C) trpm8 $^{-/-}$ mPKs (n = 35) vs. WT mPKs (n = 27) and in (F) eTRPM8 HaCaT cells (n = 15) vs. CTL HaCaT cells (n = 16). Immunodetection (G) of overexpressed eTRPM8 (green) in HaCaT cells expressing a DsRed targeted to mitochondria (red) illustrates that eTRPM8-expressing ER microdomains are in close proximity to mitochondria. (G, Right) Enlarged image of the boxed region. (H and I) Coordinated motility confirms tight coupling between eTRPM8-enriched ER elements and mitochondria in HaCaT cells. The ER elements were either stained with Brefeldin A BODIPY 558/568 (H) or identified by mTurquoise2 (mTq2) fluorescence, following eTRPM8-mTq2 expression (I). The mitochondria (H and I) were stained with either MitoTracker Green FM (MTG) or MitoTracker Red FM (MTR), respectively. Spatial distribution of the ER elements and mitochondria was analyzed using x-y time series confocal imaging. The galleries (H and I, Upper Right) show enlarged images of Brefeldin A BODIPY and MTG fluorescence (H) or mTq2 and MTR fluorescence (I) captured from the boxed region (H and I, Upper Left) and their overlays, as indicated. Motility analysis was conducted for the outlined (magenta ellipses) mitochondrion and the adjacent ER element. The x and y positions of the local maxima of the MTG and Brefeldin A BODIPY fluorescence (H) or mTq2 and MTR fluorescence (I) were computed and plotted over time. The 3D plots (H and I,

eTRPM8 Facilitates Mitochondrial ATP Synthesis at 37 °C and Adjusts ATP Production to Mild-Cold Adaptation Requirements.

In pancreatic and hepatic cells, a correlated Ca^{2+} oscillation in both cytosol and mitochondria has been shown to support a cell-specific pacing of metabolism, which coordinates with cell function (28–30). Mitochondrial Ca^{2+} transients have been reported to increase mitochondrial dehydrogenase (DHase) activity that in turn enhances ATP synthesis. In addition, three key DHases of the tricarboxylic acid (TCA) cycle have been reported to be Ca^{2+} dependent, suggesting that mitochondrial Ca^{2+} regulates the NADH/NAD$^+$ ratio, which in turn controls ATP synthesis (31–33). We therefore tested whether eTRPM8 expression and activity may influence ATP synthesis in keratinocytes. The eTRPM8 KD HaCaT cells showed almost 40% decrease of steady-state $[Ca^{2+}]_m$ (Fig. 4A), which correlates with a 40% fall in steady-state $[ATP]_m$ detected with mitochondrial luciferase (Fig. 4B). Mitochondrial ATP is thought to represent between 40% and 60% of total cell ATP, depending on cell model and physiology. We therefore expected that the eTRPM8-dependent mitochondrial ATP synthesis would have a global impact on cell energy stores. Consistent with this, measurements of total intracellular ATP content ($[ATP]_i$) in the eTRPM8 KD HaCaT cells and mPKs from trpm8$^{-/-}$ mice revealed a significant decrease compared with that in the respective controls (Fig. 4 C and D, Left).

Apart from being involved in all energy-dependent cellular processes, ATP is excreted as paracrine/autocrine messenger, which may contribute to EH. Indeed, purinergic receptors are expressed in the plasma membrane of keratinocytes and their activation modulates proliferation (34). Bearing this in mind, we measured extracellular ATP concentration ($[ATP]_e$) and, as in the case of $[ATP]_i$, detected $[ATP]_e$ decrease with both the KD HaCaT cells and mPKs from trpm8$^{-/-}$ mice (Fig. 4 C and D, Right). This revealed that $[ATP]_e$ represents a good correlate of $[ATP]_i$. Altogether these data demonstrate that eTRPM8 is involved in modulation of mitochondrial ATP synthesis that defines both intra- and extracellular ATP concentration at 37 °C.

As eTRPM8 is a cold sensor, we tested whether mild cold could stimulate ATP production. The notion that ATP production could be enhanced by cold seems to be counterintuitive, because it is well appreciated that the optimal temperature for enzyme activity is 37 °C. To verify whether keratinocyte metabolism is sensitive to acute and chronic cold as expected, we assessed the temperature dependence of the total DHase activity in hNEKs and found that total DHase activity is gradually reduced during acute cooling for 1 h (Fig. 4E). Conversely, keratinocyte acclimatization to cold within 24 h prior to measuring total DHase activity at 37 °C revealed no difference in DHase activity in keratinocytes grown at 37 °C. This suggests that intrinsic temperature dependence of the enzyme activity dominates and masks a much weaker, if any, effect of the keratinocyte adaptation on DHase activity (i.e., increased expression, protein modifications increasing activity). We therefore assessed ATP content in the culture medium of control HaCaT cells grown at temperatures of 37 °C, 31 °C, and 25 °C for 24 h. This revealed no statistically significant alterations of $[ATP]_e$ (Fig. 4F), which is hardly consistent with the notion of decreased global metabolism at lowered temperatures. Overexpression of eTRPM8 increased $[ATP]_e$ relative to control HaCaT cells at all tested temperatures, whereas eTRPM8 knockdown (shM8) had an opposite effect. It is noteworthy that overexpression of the eTRPM8 pore-killer mutant [eTRPM8(Y148A)] reversed the effect observed

Lower Left) show the trajectory of the motion of the mitochondrion (H, green; I, red) and adjacent (H, red) ER element or (I, blue) eTRPM8-enriched ER element. The x and y positions of the organelles in time are seen in the x-y and x-z projections on the 3D plot, respectively. The x vs. x and y vs. y positions for the mitochondrion and the ER element are plotted (H and I, Lower Center and Lower Right, respectively). Linear regression analysis revealed high correlation between the parameters in all four cases: R = 0.973 (H, Lower Center), R = 0.970 (H, Lower Right), R = 0.963 (I, Lower Center), and R = 0.967 (I, Lower Right).
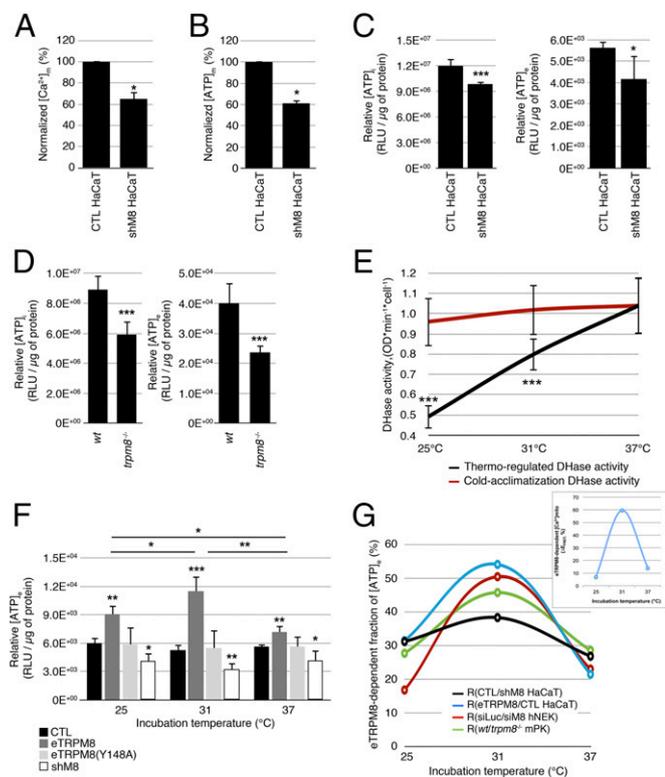
Fig. 4. eTRPM8 conveys cold-dependent enhancement of ATP synthesis. (*A*) A steady-state $[Ca^{2+}]_m$ was assessed using mtAEQmut probe in control and eTRPM8 KD HaCaT cells (CTL HaCaT and shM8 HaCaT, respectively). Bar diagram plot compares mean ± SEM values in CTL HaCaT cells (*n* = 13) and ShM8 HaCaT cells (*n* = 11) in three independent experiments, after rescaling the mean control value to 100%. (*B*) Basal ATP concentration within mitochondria ($[ATP]_m$) was measured with mitochondria targeted ATP-dependent luciferase in CTL HaCaT (*n* = 12) and shM8 HaCaT (*n* = 12) cells at 37 °C. Decrease of $[ATP]_m$ in shM8 HaCaT cells (presented as percentage of control) is summarized in the bar diagram plot. (*C*) Intracellular and extracellular ATP concentrations ($[ATP]_i$ and $[ATP]_e$) were quantified using luciferase assay (*Materials and Methods*) in CTL HaCaT and shM8 HaCaT cells at 37 °C and compared (*n* = 5). (*D*) The same as *C* but for mPKs from WT and $trpm8^{-/-}$ mice (*n* = 5). (*E*) Dehydrogenase (DHase) activity assay performed at 37 °C, 31 °C, or 25 °C demonstrates strong temperature dependence of DHase activity in hNEKs cultured at 37 °C (black curve, thermo-regulated DHase activity). No significant deviations in DHase activity associated with cold acclimatization of hNEKs cultured at 37 °C, 31 °C, or 25 °C were detected by DHase assay performed at 37 °C (red curve, cold acclimatization DHase activity). *n* = 3. (*F*) Quantification of $[ATP]_e$ HaCaT cells cultured at 37 °C, 31 °C, or 25 °C for 24 h following transfection with either vector (CTL), eTRPM8, pore-killer mutant eTRPM8(Y148A), or shRNA targeting eTRPM8 (shM8). *n* = 5. (*G*) Contribution of eTRPM8 to regulation of ATP synthesis was estimated from TRPM8-dependent fraction of $[ATP]_e$: (*i*) the differences between WT/CTL/siLuc and KO/shM8/siTRPM8 $[ATP]_e$ values were divided by corresponding WT/CTL/siLuc $[ATP]_e$ values, for mPKs, HaCaT cells, and hNEKs, respectively and (*ii*) the difference between eTRPM8 HaCaT and CTL HaCaT $[ATP]_e$ values was divided by the eTRPM8 HaCaT $[ATP]_e$ value. (*Inset*) Using the same strategy the eTRPM8-dependent component of a steady-state $[Ca^{2+}]_m$ was assessed by the measurements of 4mTM3cpv Cameleon FRET efficacy (E_{FRET}) in HaCaT and eTRPM8 HaCaT cells. Smooth curves show parabolic interpolation of the mean values (*n* = 5). Note that in all cases, an impact of eTRPM8 activity on $[ATP]_e$ is maximal around 31 °C. Also note correlation between eTRPM8-dependent $[Ca^{2+}]_m$ and $[ATP]_e$.

with overexpression of functional eTRPM8, suggesting that eTRPM8 channel activity is required for full-scale ATP production, especially under mild-cold conditions. Nevertheless, the $[ATP]_e$ levels, observed in control HaCaT cells and following eTRPM8 (Y148A) expression, were not statistically different, suggesting that the mutant is not negative dominant (Fig. 4*F*). Unexpectedly, $[ATP]_e$ in control mPKs gradually decreased with cooling and was

reduced in mPKs from $trpm8^{-/-}$ mice with a maximal drop (about 50%) at 31 °C (Fig. S5*A*). In contrast, $[ATP]_e$ in hNEKs increased with cooling at 31 °C and was reduced by siTRPM8 expression (Fig. S5*B*). Thus, all cell models tested support the notion that eTRPM8 is involved in control of ATP synthesis. Despite the difference in temperature dependence of $[ATP]_e$ in different cell models, reflecting some contribution of eTRPM8-independent mechanisms, the impact of eTRPM8 on ATP synthesis was always maximal around 31 °C (Fig. 4*G*) and correlated with an eTRPM8-dependent fraction of $[Ca^{2+}]_m$ (Fig. 4*G*, *Inset*). Although an increase in the eTRPM8-dependent fraction of $[ATP]_e$ at 31 °C can be attributed to elevation of the mitochondrial ATP synthesis boosted by the uptake of Ca^{2+} released from the ER via activated eTRPM8, subsequent decrease of this fraction at 25 °C cannot be explained by temperature dependence of TRPM8 and likely reflects an intrusion of a different mechanism, which decreases ATP synthesis despite elevated mitochondrial Ca^{2+} uptake. One of the possible candidates for such a mechanism is mitochondrial superoxide ($O_2^{\bullet-}$) production, which was reported to correlate well with metabolic rate (35, 36). It should be emphasized that keratinocytes are more prone to $O_2^{\bullet-}$ accumulation than other cell types due to reduced superoxide dismutase (SOD) activity (37).

eTRPM8 Activation Facilitates Superoxide Production in Mitochondria and Triggers Its Accumulation Under Mild-Cold Conditions. To test the above hypothesis we compared mitochondrial $O_2^{\bullet-}$ accumulation in response to eTRPM8 stimulation with 10 μM icilin in control (Fig. 5*A*) and eTRPM8-overexpressing (Fig. 5*B*) HaCaT cells and in WT mPKs and mPKs from $trpm8^{-/-}$ mice (Fig. S6*A*), using *x*-*y* time series confocal imaging of MitoSOX Red fluorescence in the living cells (*Materials and Methods*). This revealed that $O_2^{\bullet-}$ accumulation was augmented in eTRPM8-overexpressing HaCaT cells and was suppressed in mPKs from $trpm8^{-/-}$ mice. Indeed, the mean rate of $O_2^{\bullet-}$ accumulation, estimated as mass of MitoSOX fluorescent signal per second following icilin application, was found to be 9 times higher in eTRPM8-overexpressing HaCaT than control HaCaT cells (Fig. 5*C*) and 7.5 times lower in mPKs from $trpm8^{-/-}$ mice than in WT mPKs (Fig. 5*D*).

As natural stimulus-activating TRPM8 is cold, and because long-term incubation of keratinocytes in mild-cold conditions affects the ATP content (see above), we also tested the effect of long-term cooling on $O_2^{\bullet-}$ accumulation in different keratinocyte models, using CellRox Deep Red Reagent, a nonspecific reactive oxygen species (ROS) probe, previously reported to be confined to the cytosol. In contrast to that reported previously, we found that this probe accumulates in mitochondria, because it was colocalized with mitochondria-targeted GFP (Fig. S6*B*). Furthermore, we detected that CellRox Deep Red Reagent fluorescence decreased with increasing concentration of hydrogen peroxide, H_2O_2 (Fig. S6*C*). This indicates that an increase in the intensity of CellRox fluorescence is not a reporter of $-H_2O_2$ accumulation. On the other hand, a 30-min pretreatment of keratinocytes with MnTBAP, a superoxide ($O_2^{\bullet-}$) and peroxynitrite ($ONOO^-$) scavenger, results in strong decrease of CellRox fluorescence. Because peroxynitrites are down-products of $O_2^{\bullet-}$ (38, 39), CellRox Deep Red Reagent seems to be a good reporter of the $O_2^{\bullet-}$ catalytic chain activity in mitochondria. Bearing this in mind, we assessed steady-state superoxide concentration $[O_2^{\bullet-}]$ in living hNEKs (Fig. 5*E*) or HaCaT cells (Fig. 5*F*) after 72-h or 24-h culturing at 37 °C, 31 °C, or 25 °C. The hNEKs were transfected either with control siRNA (siLuc) or with siRNA targeting the pore-encoding sequence of TRPM8 (siTRPM8), whereas HaCaT cells were transfected with empty vector (CTL), eTRPM8 plasmid, or eTRPM8 + SOD1 plasmids. Imaging of CellRox Deep Red fluorescence was performed using a confocal microscope equipped with a CO_2 incubator. The $O_2^{\bullet-}$-specific signals (*Materials and Methods*) obtained under different siRNA conditions were normalized to those in corresponding controls (37 °C; hNEKs, transfected with siLuc, or HaCaT cells, transfected with empty vector) and compared. This revealed that transfection of hNEKs with siRNA targeting the pore-encoding sequence of TRPM8 partially but significantly
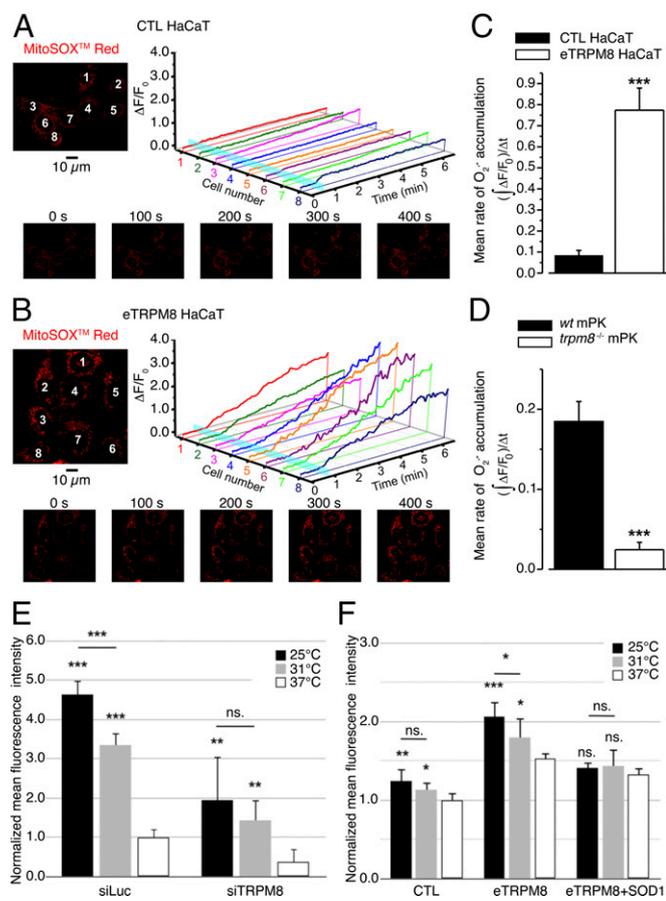
Fig. 5. Icilin- and cold-induced $O_2^{\bullet-}$ accumulation depends on the level of eTRPM8 expression. (*A* and *B*) Confocal images of MitoSOX Red fluorescence revealed distinct mitochondrial staining in control HaCaT cells, CTL HaCaT (*A*), and HaCaT cells overexpressing epithelial TRPM8, eTRPM8 HaCaT (*B*). Changes in the MitoSOX fluorescence in response to stimulation with 10 μM icilin were monitored using the *x-y* time series imaging protocol. The MitoSOX fluorescence intensity (*F*) was normalized to the averaged fluorescence intensity before agonist application (F_0). In *A* and *B*, relative changes in the fluorescence intensity ($\Delta F/F_0$), averaged within each of eight cells denoted by the numbers on the images (*Upper Left*), are plotted over time, respectively (*Upper Right*). Icilin application is depicted by a vertical cyan bar. The galleries (*A* and *B*, *Lower*) show the images of MitoSOX fluorescence captured at times indicated above the images. Mean rates of $O_2^{\bullet-}$ accumulation were estimated as masses of MitoSOX fluorescent signal per second following icilin application, $(\int \Delta F/F_0)/\Delta t$, in CTL HaCaT (*n* = 28), in eTRPM8 HaCaT (*n* = 20), in primary cultures of either WT mouse keratinocytes (WT mPK) (*n* = 8) or *trpm8*$^{-/-}$ mouse keratinocytes (*trpm8*$^{-/-}$ mPK) (*n* = 10), and compared in *C* and *D*, respectively. (*E*) Steady-state superoxide concentration [$O_2^{\bullet-}$] was assessed in living hNEKs after 72 h culturing at 37 °C, 31 °C, or 25 °C, using CellRox Deep Red Reagent. Cells were transfected either with control siRNA (siLuc) or with siRNA targeting the pore-encoding sequence of TRPM8 (siTRPM8). For each temperature and siRNA condition the measurements were performed in three Petri dishes, sequentially mounted on the microscope stage at the ambient temperature corresponding to the preincubation temperature. In each Petri dish confocal imaging of CellRox Deep Red fluorescence was performed from four fields of view, 230 × 230 μm (1,024 × 1,024 pixels) each. The $O_2^{\bullet-}$-specific increases in the CellRox Deep Red signal mass (*Materials and Methods*) for each condition were averaged, normalized to the mean value detected at 37 °C in siLuc-transfected hNEKs, and compared. (*F*) The same as *E*, but for HaCaT cells transfected with empty vector (CTL), eTRPM8 plasmid, or eTRPM8 + SOD1 plasmids and cultured for 24 h at 37 °C, 31 °C, or 25 °C. The data were normalized to the mean value detected at 37 °C in HaCaT cells transfected with empty vector and compared. Note that the differences between corresponding values for different expression conditions (*E* and *F*) are statistically significant at all three temperatures tested with *P* < 0.05. Experiments in *E* and *F* were performed three times and include more than 200 cells per experiment.

suppresses $O_2^{\bullet-}$ accumulation at all three temperatures tested (Fig. 5*E* and Fig. S6*E*). Bearing in mind that $O_2^{\bullet-}$ content depends on both its synthesis and dismutation by superoxide dismutases, we tested in HaCaT cells whether the effect of eTRPM8 overexpression can be reversed by overexpression of the Cu/Zn superoxide dismutase (SOD1). This revealed that significant increase of $O_2^{\bullet-}$ accumulation caused by eTRPM8 overexpression at all temperatures tested was partially reversed by concomitant overexpression of SOD1 (Fig. 5*F*). Furthermore, SOD1 overexpression suppresses cold dependence of $O_2^{\bullet-}$ accumulation, thus suggesting that the balance between $O_2^{\bullet-}$ dismutation and synthesis remains the same regardless of the temperature. However, simultaneous overexpression of eTRPM8 and SOD1 resulted in a small but significant increase of $O_2^{\bullet-}$ accumulation relative to cells transfected with empty vector (CTL) at all tested temperatures. This suggests that, with gradual cooling, elevation of eTRPM8 activity progressively overrides a native SOD activity, whereas when SOD1 is overexpressed, a cold-dependent increase of TRPM8 activity is masked.

Altogether, our data demonstrate that activation of eTRPM8 in the ER leads to the increase of $[Ca^{2+}]_m$ that consequently enhances ATP and $O_2^{\bullet-}$ production in mitochondria. In line with this, 24–72 h incubation of keratinocytes under mild-cold conditions elevates both $[ATP]_i$ and $[O_2^{\bullet-}]_i$. These findings are of great physiological importance, because ATP has been reported to be a key inducer of keratinocyte proliferation, whereas $O_2^{\bullet-}$ is involved in keratinocyte differentiation. Indeed, SOD1 was shown to be expressed in the basal layer, but to disappear in differentiated layers of epidermis (40). Based on this observation the authors speculated that in proliferating keratinocytes (which have elevated energy metabolism) SOD1 serves to maintain $O_2^{\bullet-}$ at a low level and, thereby, to protect the cells from oxidation, whereas in differentiated cells (which have low energy metabolism) enhanced accumulation of $O_2^{\bullet-}$ and perhaps peroxinitrites, resulting from down-regulation of SOD1, may be involved in regulation of keratinocyte differentiation. The latter was further supported by observation of correlation between ROS concentration and degree of keratinocyte differentiation (41, 42). We therefore hypothesized that eTRPM8-dependent production of both ATP and $O_2^{\bullet-}$ may control the proliferation/differentiation balance of keratinocytes.

eTRPM8 Regulates Proliferation in a Temperature-Dependent Manner.
To test whether background, nonstimulated eTRPM8 activity at 37 °C is relevant to EH, hNEKs transfected with either control siRNA or anti-TRPM8 siRNA were subjected to a growth assay at 37 °C. The eTRPM8 KD hNEKs showed reduced growth rate in virtual absence of apoptosis (less than 1%), suggesting that lack of eTRPM8 suppresses proliferation (Fig. 6*A*). Assessment of thermosensitivity of keratinocyte proliferation revealed that control HEKs showed gradual decrease of growth rate with cooling, as expected, whereas eTRPM8 knockdown reduces the proliferation rate only at 37 °C (Fig. 6*B*), consistent with the notion that eTRPM8 activity at 37 °C encourages proliferation. eTRPM8 overexpression did not modify the growth at 37 °C, but significantly suppressed it at 25 °C. The latter was reversed by concomitant overexpression of SOD1, thus suggesting that the effect was mediated by $O_2^{\bullet-}$ (Fig. 6 *B* and *C*, *Center* and *Right*). Conversely, eTRPM8+SOD1 cotransfection reduced proliferation at both 37 °C and 31 °C, compared with control and eTRPM8-overexpressing cells. Paradoxically, even though eTRPM8+SOD1-overexpressing cells had higher ATP content than both control cells and eTRPM8-overexpressing cells at 37 °C (Fig. 6*C*, *Left*), their growth rate was significantly reduced (Fig. 6*C*, *Right*).

To assess the extent of eTRPM8 recruitment to keratinocyte proliferation in vivo, we examined whether cold/menthol stimulation of mouse epidermis would affect cell proliferation in SB. As most of mouse skin is protected from variations of ambient temperature by fur, which acts as a thermal insulator, we shaved the two sides of mice but kept the fur on the back, as a control. We applied 1 mM of menthol twice a day for 3 wk on the right side, whereas the left side remained untreated. Furred back skin was shaved after mice were euthanized, and three skin samples were
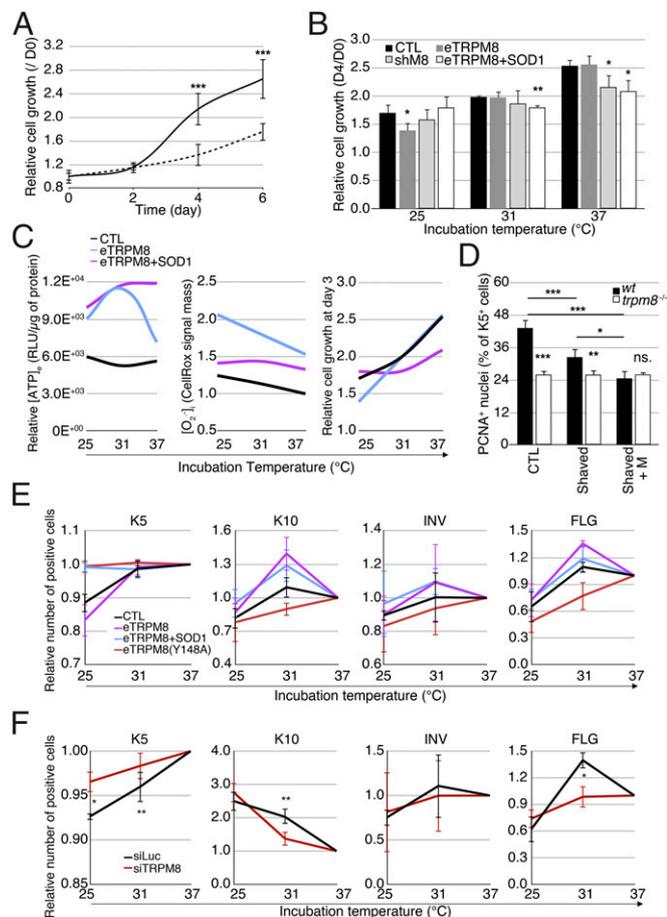
Fig. 6. Mild cold suppresses proliferation and facilitates differentiation of keratinocytes in an eTRPM8-dependent manner. (*A*) The graph illustrates growth of induced (*Materials and Methods*) hNEKs transfected with either control siRNA (black solid line) or anti-TRPM8 siRNA (dashed line) during 6 d. Data are presented as fold increase of the cell number from day 0. $n = 3$. (*B*) Bar diagram plot compares growth of HaCaT cells transfected with empty vector (CTL), eTRPM8 vector (eTRPM8), or shRNA anti-TRPM8 vector (shM8) or cotransfected with eTRPM8 and SOD1 vectors (eTRPM8+SOD1) at 25 °C, 31 °C, and 37 °C. $n = 3$. (*C*) Charts illustrate dependence of [ATP]$_e$ (*C, Left*), [O$_2^{•-}$]$_i$ (*C, Center*), and cell growth (*C, Right*) on ambient temperature for HaCaT cells transfected with either empty vector (CTL) or eTRPM8 vector (eTRPM8) or cotransfected with eTRPM8 and SOD1 vectors (eTRPM8+SOD1). Smooth curves are the result of parabolic interpolation of the mean values ($n = 3$). (*D*) Count of PCNA-positive nuclei in basal epidermis compartment was performed on slices from three different areas of skin (*Materials and Methods*): furred (CTL), shaved (Shaved), and shaved with application of 1 mM Menthol twice a week (Shaved+M). Six WT and seven *trpm8*$^{-/-}$ mice were treated for 3 wk before analysis was commenced. Bar diagram plot shows the ratio of the number of PCNA-positive cells divided by the number DAPI-positive nuclei in the basal compartment identified with anti-keratin 14 antibodies. (*E*) Distribution of keratinocyte phenotypes of HaCaT cells induced at 37 °C, 31 °C, or 25 °C for 24 h was measured with flow cytometry and compared for HaCaT cells transfected with empty vector (CTL), eTRPM8 vector (eTRPM8), or eTRPM8 mutant vector [eTRPM8(Y148A)] or cotransfected with eTRPM8 and SOD1 vectors (eTRPM8+SOD1). The distribution of keratinocyte phenotypes was estimated on the basis of the percentage of cells expressing basal differentiation marker, K5; early spinal differentiation marker, K10; late spinal differentiation marker, INV; and granular differentiation marker, FLG. Cold dependency of keratinocyte differentiation was calculated with normalization of values from cells grown at 25 °C and 31 °C by values from cells grown at 37 °C. Data are presented as mean ± SD ($n = 3$). Statistical significance was calculated for eTRPM8, eTRPM8+SOD1, and eTRPM8(Y148A) compared with control cells. (*F*) Same as *E* but for hNEKs transfected with either control siRNA (siLuc) or anti-TRPM8 siRNA (siTRPM8) for 4 d. Experiments in *E* and *F* were performed three times and include more than 100,000 cells per experiment. Data are presented as mean ± SD.

compared: control (from the back), shaved (from the left side), and menthol-treated shaved (from the right side). Immunohisto-fluorescence detection of K14-positive cells, which form the basal transit amplifying compartment of epidermis cells (43), and PCNA-positive cells, which reflect the cell population undergoing the cell cycle, was performed with a confocal microscope. The proliferation rate was then estimated by dividing the number of PCNA$^+$/K14$^+$ cells by the number of PCNA$^-$/K14$^+$ cells. In control conditions (unshaved mice), this ratio was significantly reduced in *trpm8*$^{-/-}$ epidermis, which reveals a TRPM8-dependent, cold-independent regulatory component of keratinocyte proliferation. We also detected a significant decrease of this ratio in shaved *trpm8*$^{+/+}$ epidermis and its further reduction in shaved *trpm8*$^{+/+}$ epidermis subjected to menthol treatment (Fig. 6*D*), which demonstrates that cooling reduces proliferation in vivo. It should be emphasized that in all skin samples from *trpm8*$^{-/-}$ mice this ratio was reduced to the same extent, independently of shaving and menthol treatment. This result suggests that the decrease of the keratinocyte proliferation rate in vivo in response to cooling cannot be explained solely by customary temperature dependence of metabolic rate. Altogether, these results confirm that in vivo mild cold reduces the number of proliferating keratinocytes in an eTRPM8-dependent manner. Nevertheless, variations in the number of PCNA$^+$ cells can be explained by either slowing down of the cell cycle or an increase of proliferation rate. The effect of eTRPM8 knockdown in HaCaT cells at 37 °C on cell growth (Fig. 6*B*) undoubtedly favors the second hypothesis and confirms that eTRPM8 expression is required for full-scale proliferation of basal keratinocytes at 37 °C and that mild cold reduces the proliferation rate of keratinocytes in a TRPM8-dependent manner. Regardless of the mechanism linking eTRPM8 expression to full-scale keratinocyte proliferation, reduction of keratinocyte proliferation rate may involve two different mechanisms: cell cycle arrest associated with quiescence phase or induction of differentiation.

Stimulation of eTRPM8 with Mild Cold Induces Keratinocyte Differentiation. Upon quantification of the differentiation rate in 2D cultures of keratinocytes several issues have to be taken into account. First, it relies on the assumption that the initial proportion of different keratinocyte phenotypes (basal, spinous, granular, corneocytes) is well defined and constant in all Petri dishes. Second, induced changes in the proportion of the keratinocyte phenotypes, interpreted as differentiation, are generally assessed with a Western blot. This procedure, however, gives information on the total expression of the so-called differentiation markers in the cell population, but does not provide any information on either the number of cells in each phenotype or the mean expression level of differentiation markers in single cells. Third, on many occasions, quantification of the differentiation rate is based on detection of early differentiation markers only. Therefore, to quantify eTRPM8-linked cold dependency of the keratinocyte differentiation, we recently showed the efficiency of flow cytometry (24), as in the case of keratinocytes freshly isolated from mouse skin (Fig. 2*G*). Although the experiments were conducted with simultaneous detection of two of four markers (Fig. S7), to simplify visualization, the data are presented in charts showing the relative proportion of cells expressing one marker. Surprisingly, about 90% of cultured keratinocytes revealed the expression of basal markers K5 and K14, whereas less than 10% of the cells expressed differentiation markers K10 and INV. This could explain why we failed to detect any specific alterations of basal marker expression in HaCaT cells (Fig. 6*E*) and hNEKs (Fig. 6*F*) incubated at 31 °C, even though when cells were incubated at 25 °C, a significant decrease in the expression of these markers was observed. Intriguingly, in the case of eTRPM8 overexpression there were more K10-positive HaCaT cells at 37 °C than at 31 °C, whereas in the case of concomitant overexpression of SOD1 the situation was the opposite. This suggests a permissive role of O$_2^{•-}$ in early differentiation. This hypothesis is supported by the observation that progressive cooling causes a gradual increase of K10 expression in hNEKs, which are known to express endogenous SOD1 at

an early stage of differentiation. Expression of the late SS and SG INV marker was found to be weakly dependent on eTRPM8 expression and stimulation with mild cold. In contrast, the size fraction of cells with the granular marker, FLG, depended strongly on eTRPM8 expression/activity and showed a bell-shaped cold sensitivity with an optimum at the human physiological skin temperature of about 31 °C. Note that this bell-shaped cold sensitivity in the eTRPM8-overexpressing HaCaT cell population is identical to that of hNEKs. Furthermore, this cold sensitivity correlates with the cold sensitivity of ATP synthesis, suggesting that terminal differentiation of keratinocytes is a highly ATP-dependent process. These data together demonstrate that eTRPM8 is involved in the differentiation of keratinocytes not only in mouse (Fig. 2*G*) but also in human (Fig. 6 *E* and *F*) epidermis and conveys cold sensitivity of this process.

In conclusion, we have characterized a new archetype of the TRP channel encoded by a single gene. This channel is a TRPM8 isoform expressed in the endoplasmic reticulum of keratinocytes and serves as a central element of signaling pathways engaged in cold sensitivity of EH. Our results revealed a key role of eTRPM8 in keratinocyte bioenergetics: arbitration of the keratinocyte proliferation/differentiation balance (within the range of mild cold temperatures) via orchestrating the $Ca^{2+}/ATP/O_2^{\bullet-}$ triad (Fig. S8 and *SI Results and Discussion*). This eTRPM8-mediated temperature-dependent energy metabolism and signaling in keratinocytes might provide skin with the capacity to adapt to large variations of environmental temperature.

Materials and Methods

Cell Culture. See *SI Materials and Methods*.

Establishment of *trpm8*^−/− Mice. To suppress ion channel activity of every channel-like TRPM8 isoform, we inserted LoxP sites with homologous recombination in introns 17 and 20. This ultimately led to a 2,500-bp deletion including exons 18–20, which encode transmembrane domains 3–5 in addition to the first part of the P loop of the TRPM8 channel. Please refer to *SI Materials and Methods* for extended description of the methods. This study was carried out in strict accordance with the French Law (Articles R214-117 to 121 of the rural code) and recommendations in the Guide for the Care and Use of Laboratory Animals (www.recherche-animale.org).

Molecular Biology and Biochemistry. See *SI Materials and Methods* and Table S1.

Electrophysiology. See *SI Materials and Methods*.

Visualization of the ER and Mitochondria. See *SI Materials and Methods*.

Visualization of Agonist-Induced Changes of Ca^{2+} Concentration in Cytosol ($[Ca^{2+}]_c$) and Mitochondria ($[Ca^{2+}]_m$). Changes of $[Ca^{2+}]_c$ and $[Ca^{2+}]_m$ were imaged using the high-affinity fluorescent Ca^{2+} indicator fluo-4 and Ca^{2+} indicator rhod-2. Mitochondrial Ca^{2+} signal was also evaluated 48 h after transfection of M8-CTL and M8-KD cells with an adenoviral mutated mitochondria-targeted aequorin probe (mtAEQmut). For extended procedures, refer to *SI Materials and Methods*.

Superoxide Assessment. Steady-state superoxide concentration $[O_2^{\bullet-}]$ was assessed in living hNEKs or HaCaT cells after 72 h or 24 h culturing at 37 °C, 31 °C, or 25 °C, using CellRox Deep Red Reagent (Molecular Probes), loaded by 30-min incubation of the cells with 2.5 μM of the dye at 37 °C. Please refer to *SI Materials and Methods* for extended description of the methods.

Time domain–fluorescence lifetime imaging microscopy (TM-FLIM) was achieved to estimate the difference in steady-state $[Ca^{2+}]_m$ with a Cameleon bioindicator. For details, see *SI Materials and Methods*.

Data Analysis and Statistical Procedures. Each experiment was repeated at least three times independently. Data are expressed as mean ± SD when not indicated in legends. The data were analyzed and graphs plotted using Origin 5.0 software (Microcal). InStat3 (GraphPad Software) was used for statistical analysis and the mean values were compared using either an unpaired *t* test with Welch's corrected test (two groups) or a one-way ANOVA with a Dunnett multiple-comparison posttest (three or more groups). Statistical significances were as follows: *$P < 0.05$, **$P < 0.01$, and ***$P < 0.001$. Smooth curves on the graphs were obtained by interpolation of data points, using a parametric Lagrange second-degree polynomial: parabola for interpolation of three data points.

1. Fuchs E (1990) Epidermal differentiation: The bare essentials. *J Cell Biol* 111(6 Pt 2): 2807–2814.
2. Smith AD, Crabtree DR, Bilzon JL, Walsh NP (2010) The validity of wireless iButtons and thermistors for human skin temperature measurement. *Physiol Meas* 31(1):95–114.
3. Lumpkin EA, Caterina MJ (2007) Mechanisms of sensory transduction in the skin. *Nature* 445(7130):858–865.
4. Caterina MJ, Julius D (2001) The vanilloid receptor: A molecular gateway to the pain pathway. *Annu Rev Neurosci* 24:487–517.
5. McKemy DD, Neuhausser WM, Julius D (2002) Identification of a cold receptor reveals a general role for TRP channels in thermosensation. *Nature* 416(6876):52–58.
6. Peier AM, et al. (2002) A TRP channel that senses cold stimuli and menthol. *Cell* 108(5): 705–715.
7. Story GM, et al. (2003) ANKTM1, a TRP-like channel expressed in nociceptive neurons, is activated by cold temperatures. *Cell* 112(6):819–829.
8. Kwan KY, et al. (2006) TRPA1 contributes to cold, mechanical, and chemical nociception but is not essential for hair-cell transduction. *Neuron* 50(2):277–289.
9. Obata K, et al. (2005) TRPA1 induced in sensory neurons contributes to cold hyperalgesia after inflammation and nerve injury. *J Clin Invest* 115(9):2393–2401.
10. Mandadi S, et al. (2009) TRPV3 in keratinocytes transmits temperature information to sensory neurons via ATP. *Pflugers Arch* 458(6):1093–1102.
11. Koizumi S, et al. (2004) Ca2+ waves in keratinocytes are transmitted to sensory neurons: The involvement of extracellular ATP and P2Y2 receptor activation. *Biochem J* 380(Pt 2):329–338.
12. Gifford JR, Heal C, Bridges J, Goldthorpe S, Mack GW (2012) Changes in dermal interstitial ATP levels during local heating of human skin. *J Physiol* 590(Pt 24): 6403–6411.
13. Moqrich A, et al. (2005) Impaired thermosensation in mice lacking TRPV3, a heat and camphor sensor in the skin. *Science* 307(5714):1468–1472.

14. Peier AM, et al. (2002) A heat-sensitive TRP channel expressed in keratinocytes. *Science* 296(5575):2046–2049.
15. Cheng X, et al. (2010) TRP channel regulates EGFR signaling in hair morphogenesis and skin barrier formation. *Cell* 141(2):331–343.
16. Denda M, Tsutsumi M, Denda S (2010) Topical application of TRPM8 agonists accelerates skin permeability barrier recovery and reduces epidermal proliferation induced by barrier insult: Role of cold-sensitive TRP receptors in epidermal permeability barrier homoeostasis. *Exp Dermatol* 19(9):791–795.
17. Bautista DM, et al. (2007) The menthol receptor TRPM8 is the principal detector of environmental cold. *Nature* 448(7150):204–208.
18. Dhaka A, et al. (2007) TRPM8 is required for cold sensation in mice. *Neuron* 54(3): 371–378.
19. Bidaux G, et al. (2007) Prostate cell differentiation status determines transient receptor potential melastatin member 8 channel subcellular localization and function. *J Clin Invest* 117(6):1647–1657.
20. Bidaux G, et al. (2005) Evidence for specific TRPM8 expression in human prostate secretory epithelial cells: Functional androgen receptor requirement. *Endocr Relat Cancer* 12(2):367–382.
21. Latorre R, Brauchi S, Orta G, Zaelzer C, Vargas G (2007) ThermoTRP channels as modular proteins with allosteric gating. *Cell Calcium* 42(4–5):427–438.
22. Brauchi S, Orta G, Salazar M, Rosenmann E, Latorre R (2006) A hot-sensing cold receptor: C-terminal domain determines thermosensation in transient receptor potential channels. *J Neurosci* 26(18):4835–4840.
23. Beck B, et al. (2007) Prospects for prostate cancer imaging and therapy using high-affinity TRPM8 activators. *Cell Calcium* 41(3):285–294.
24. Borowiec AS, Delcourt P, Dewailly E, Bidaux G (2013) Optimal differentiation of in vitro keratinocytes requires multifactorial external control. *PLoS ONE* 8(10):e77507.

25. Vanden Abeele F, Roudbaraki M, Shuba Y, Skryma R, Prevarskaya N (2003) Store-operated Ca2+ current in prostate cancer epithelial cells. Role of endogenous Ca2+ transporter type 1. *J Biol Chem* 278(17):15381–15389.

26. Poburko D, Fameli N, Kuo KH, van Breemen C (2008) Ca2+ signaling in smooth muscle: TRPC6, NCX and LNats in nanodomains. *Channels* 2(1):10–12.

27. Shkryl VM, Shirokova N (2006) Transfer and tunneling of Ca2+ from sarcoplasmic reticulum to mitochondria in skeletal muscle. *J Biol Chem* 281(3):1547–1554.

28. Pralong WF, Spät A, Wollheim CB (1994) Dynamic pacing of cell metabolism by intracellular Ca2+ transients. *J Biol Chem* 269(44):27310–27314.

29. Hajnóczky G, Robb-Gaspers LD, Seitz MB, Thomas AP (1995) Decoding of cytosolic calcium oscillations in the mitochondria. *Cell* 82(3):415–424.

30. Jouaville LS, Pinton P, Bastianutto C, Rutter GA, Rizzuto R (1999) Regulation of mitochondrial ATP synthesis by calcium: Evidence for a long-term metabolic priming. *Proc Natl Acad Sci USA* 96(24):13807–13812.

31. McCormack JG, Denton RM (1980) Role of calcium ions in the regulation of intra-mitochondrial metabolism. Properties of the Ca2+-sensitive dehydrogenases within intact uncoupled mitochondria from the white and brown adipose tissue of the rat. *Biochem J* 190(1):95–105.

32. Denton RM, McCormack JG, Edgell NJ (1980) Role of calcium ions in the regulation of intramitochondrial metabolism. Effects of Na+, Mg2+ and ruthenium red on the Ca2+-stimulated oxidation of oxoglutarate and on pyruvate dehydrogenase activity in intact rat heart mitochondria. *Biochem J* 190(1):107–117.

33. Hansford RG, Zorov D (1998) Role of mitochondrial calcium transport in the control of substrate oxidation. *Mol Cell Biochem* 184(1–2):359–369.

34. Pillai S, Bikle DD (1992) Adenosine triphosphate stimulates phosphoinositide metabolism, mobilizes intracellular calcium, and inhibits terminal differentiation of human epidermal keratinocytes. *J Clin Invest* 90(1):42–51.

35. Perez-Campo R, López-Torres M, Cadenas S, Rojas C, Barja G (1998) The rate of free radical production as a determinant of the rate of aging: Evidence from the comparative approach. *J Comp Physiol B* 168(3):149–158.

36. Sohal RS, Allen RG (1985) Relationship between metabolic rate, free radicals, differentiation and aging: A unified theory. *Basic Life Sci* 35:75–104.

37. Hornig-Do HT, et al. (2007) Human epidermal keratinocytes accumulate superoxide due to low activity of Mn-SOD, leading to mitochondrial functional impairment. *J Invest Dermatol* 127(5):1084–1093.

38. Bringold U, Ghafourifar P, Richter C (2000) Peroxynitrite formed by mitochondrial NO synthase promotes mitochondrial Ca2+ release. *Free Radic Biol Med* 29(3–4):343–348.

39. Radi R, Cassina A, Hodara R, Quijano C, Castro L (2002) Peroxynitrite reactions and formation in mitochondria. *Free Radic Biol Med* 33(11):1451–1464.

40. Carraro C, Pathak MA (1988) Characterization of superoxide dismutase from mammalian skin epidermis. *J Invest Dermatol* 90(1):31–36.

41. Tamiji S, et al. (2005) Induction of apoptosis-like mitochondrial impairment triggers antioxidant and Bcl-2-dependent keratinocyte differentiation. *J Invest Dermatol* 125(4):647–658.

42. Muramatsu S, et al. (2005) Differentiation-specific localization of catalase and hydrogen peroxide, and their alterations in rat skin exposed to ultraviolet B rays. *J Dermatol Sci* 37(3):151–158.

43. Rangarajan A, et al. (2001) Notch signaling is a direct determinant of keratinocyte growth arrest and entry into differentiation. *EMBO J* 20(13):3427–3436.

44. Thebault S, et al. (2005) Novel role of cold/menthol-sensitive transient receptor potential melastatine family member 8 (TRPM8) in the activation of store-operated channels in LNCaP human prostate cancer epithelial cells. *J Biol Chem* 280(47):39423–39435.

45. Sakuntabhai A, et al. (1999) Mutations in ATP2A2, encoding a Ca2+ pump, cause Darier disease. *Nat Genet* 21(3):271–277.

46. Prasad V, et al. (2005) Haploinsufficiency of Atp2a2, encoding the sarco(endo)plasmic reticulum Ca2+-ATPase isoform 2 Ca2+ pump, predisposes mice to squamous cell tumors via a novel mode of cancer susceptibility. *Cancer Res* 65(19):8655–8661.

47. Robb-Gaspers LD, et al. (1998) Integrating cytosolic calcium signals into mitochondrial metabolic responses. *EMBO J* 17(17):4987–5000.

48. Robb-Gaspers LD, et al. (1998) Coupling between cytosolic and mitochondrial calcium oscillations: Role in the regulation of hepatic metabolism. *Biochim Biophys Acta* 1366(1–2):17–32.

49. Harris DA, Das AM (1991) Control of mitochondrial ATP synthesis in the heart. *Biochem J* 280(Pt 3):561–573.

50. Hubbard MJ, McHugh NJ (1996) Mitochondrial ATP synthase F1-beta-subunit is a calcium-binding protein. *FEBS Lett* 391(3):323–329.

51. Dixon CJ, et al. (1999) Regulation of epidermal homeostasis through P2Y2 receptors. *Br J Pharmacol* 127(7):1680–1686.

52. Burrell HE, et al. (2005) Human keratinocytes release ATP and utilize three mechanisms for nucleotide interconversion at the cell surface. *J Biol Chem* 280(33):29667–29676.

53. Lee WK, et al. (2001) Purinoceptor-mediated calcium mobilization and proliferation in HaCaT keratinocytes. *J Dermatol Sci* 25(2):97–105.

54. Greig AV, Linge C, Cambrey A, Burnstock G (2003) Purinergic receptors are part of a signaling system for keratinocyte proliferation, differentiation, and apoptosis in human fetal epidermis. *J Invest Dermatol* 121(5):1145–1149.

55. Inoue K, et al. (2005) Characterization of multiple P2X receptors in cultured normal human epidermal keratinocytes. *J Invest Dermatol* 124(4):756–763.

56. Thiele JJ, Hsieh SN, Briviba K, Sies H (1999) Protein oxidation in human stratum corneum: Susceptibility of keratins to oxidation in vitro and presence of a keratin oxidation gradient in vivo. *J Invest Dermatol* 113(3):335–339.

57. Bidaux G, et al. (2011) Regulation of transient receptor potential melastatin 8 (TRPM8) channel activity by its short isoforms. *J Biol Chem* 287(5):2948–2962.

58. Lesage J, Blondeau B, Grino M, Bréant B, Dupouy JP (2001) Maternal undernutrition during late gestation induces fetal overexposure to glucocorticoids and intrauterine growth retardation, and disturbs the hypothalamo-pituitary adrenal axis in the newborn rat. *Endocrinology* 142(5):1692–1702.

59. Nelson TE, Lin M, Zapata-Sudo G, Sudo RT (1996) Dantrolene sodium can increase or attenuate activity of skeletal muscle ryanodine receptor calcium release channel. Clinical implications. *Anesthesiology* 84(6):1368–1379.

60. Rohács T, Lopes CM, Michailidis I, Logothetis DE (2005) PI(4,5)P2 regulates the activation and desensitization of TRPM8 channels through the TRP domain. *Nat Neurosci* 8(5):626–634.

61. Grynkiewicz G, Poenie M, Tsien RY (1985) A new generation of Ca2+ indicators with greatly improved fluorescence properties. *J Biol Chem* 260(6):3440–3450.

62. Vanden Abeele F, et al. (2006) Functional implications of calcium permeability of the channel formed by pannexin 1. *J Cell Biol* 174(4):535–546.

63. Povstyan OV, Harhun MI, Gordienko DV (2011) Ca2+ entry following P2X receptor activation induces IP3 receptor-mediated Ca2+ release in myocytes from small renal arteries. *Br J Pharmacol* 162(7):1618–1638.

64. Chami M, Ferrari D, Nicotera P, Paterlini-Bréchot P, Rizzuto R (2003) Caspase-dependent alterations of Ca2+ signaling in the induction of apoptosis by hepatitis B virus X protein. *J Biol Chem* 278(34):31745–31755.